Nonlinear observer design on SL(3) for homography estimation by exploiting point and line correspondences with application to image stabilization

Minh-Duc Hua, Jochen Trumpf, Tarek Hamel, Robert Mahony, Pascal Morin

Nonlinear observer design on SL(3) for homography estimation by exploiting point and line correspondences with application to image stabilization ⋆

Minh-Duc Hua [a], Jochen Trumpf [c], Tarek Hamel [a,b], Robert Mahony [c], Pascal Morin [d]

[a] *I3S laboratory (Laboratoire d'Informatique, Signaux et Systèmes de Sophia Antipolis), CNRS, Université Côte d'Azur, Sophia Antipolis, France,* hua(thamel)@i3s.unice.fr

[b] *Institut Universitaire de France (IUF), Paris, France*

[c] *Research School of Engineering, Australian National University, Canberra, Australia,* Jochen.Trumpf(Robert.Mahony)@anu.edu.au

[d] *Sorbonne Université, CNRS, Institut des Systèmes Intelligents et de Robotique (ISIR), Paris, France,* pascal.morin@sorbonne-universite.fr

Abstract

Although homography estimation from correspondences of mixed-type features, namely points and lines, has been relatively well studied with algebraic approaches by the computer vision community, this problem has never been addressed with nonlinear observer paradigms. In this paper, a novel nonlinear observer on the Special Linear group $SL(3)$ applied to homography estimation is developed. The key advance with respect to similar works on the topic is the formulation of observer innovation that exploits directly point and line correspondences as input without requiring prior algebraic reconstruction of individual homographies. Rigourous observability and stability analysis is provided. A potential application to image stabilization in presence of very fast camera motion, severe occlusion, specular reflection, image blur, and light saturation is demonstrated with very encouraging results.

1 Introduction

Nonlinear observer design for systems endowed with symmetry properties (and on Lie groups in particular) is a relatively new discipline, starting with Salcudean's attitude observer on the unit quaternion group (Salcudean 1991) and subsequent contributions over the last two decades (see (Nijmeijer & (Eds.) 1999, Rehbinder & Ghosh 2003, Mahony, Hamel & Pflimlin 2008, Bonnabel, Martin & Rouchon 2008, Bonnabel, Martin & Rouchon 2009, Mahony, Trumpf & Hamel 2013) and the reference therein). Since then the interest on this research topic has never ceased to expand. Owning to their algorithmic simplicity, (provable) large domain of convergence and stability, and strong robustness, nonlinear observers have increasingly become alternative solutions to classical filtering techniques, such as extended Kalman filters, unscented Kalman filters or particle filters, for state estimation (see, e.g., (Bonnabel et al. 2009, Lageman, Trumpf & Mahony 2010, Mahony et al. 2008, Mahony et al. 2013, Barrau & Bonnabel 2017)). The classical attitude estimation problem has been addressed in early nonlinear observers on the basis of Lyapunov analysis. This problem has also been a source of inspiration for the development of recent theories on invariant or equivariant observer design for systems with symmetry (Mahony et al. 2008, Bonnabel et al. 2008, Bonnabel et al. 2009, Lageman et al. 2010, Mahony et al. 2013). For instance, complementary nonlinear attitude observers exploiting the underlying Lie group structure of the Special Orthogonal group SO(3) are derived in (Mahony et al. 2008) with proofs of almost global stability of the error system. A symmetry-preserving nonlin-

⋆ Corresponding author M.-D. Hua. *hua@i3s.unice.fr.*

[1] This research was supported by the Astrid CONGRE project (ANR-18-ASTR-0006), the FUI GreenExplorer project, the EQUIPEX Robotex project, and the *Australian Research Council* through the "Australian Centre of Excellence for Robotic Vision" CE140100016.

ear observer design based on the Cartan moving-frame method is proposed in (Bonnabel et al. 2008, Bonnabel et al. 2009), which is locally valid for arbitrary Lie groups. A gradient observer design technique for invariant systems on Lie groups is proposed in (Lageman et al. 2010), leading to almost global convergence provided that a non-degenerate Morse-Bott cost function is used. An equivariant observer design method directly on the homogeneous output space for the kinematics of mechanical systems is proposed in (Mahony et al. 2013), leading to autonomous error evolution and strong convergence properties.

A large body of works on nonlinear observers has been devoted to attitude observer design on the Special Orthogonal group SO(3) (see (Mahony et al. 2008, Berkane, Abdessameud & Tayebi 2017, Trumpf, Mahony, Hamel & Lageman 2012, Khosravian, Trumpf, Mahony & Hamel 2016, Zlotnik & Forbes 2017, Batista, Silvestre & Oliveira 2014) and the references therein) and to pose observer design on the Special Euclidean group SE(3) (see (Baldwin, Mahony, Trumpf, Hamel & Cheviron 2007, Izadi & Sanyal 2016, Hua, Zamani, Trumpf, Mahony & Hamel 2011, Wang & Tayebi 2017, Vasconcelos, Cunha, Silvestre & Oliveira 2010) and the references therein). Various refinements have been carried out to take particularities of the considered system and available sensors into account. For instance, some attitude observers posed on SO(3) and based on measurements of a single time-varying direction are proposed in (Trumpf et al. 2012, Lee, Leok, McClamroch & Sanyal 2007). In particular, (Trumpf et al. 2012) exhibits some explicit persistence of excitation conditions guaranteeing the observability and asymptotic convergence of the proposed observer. Velocity-aided attitude observers developed in (Hua 2010, Martin & Salaün 2008, Roberts & Tayebi 2011) no longer rely on the assumption of weak accelerations commonly used in conventional algorithms that involve only measurements of an Inertial Measurement Unit (IMU) and a magnetometer (e.g., (Mahony et al. 2008)). Time delay in output measurements is considered in (Khosravian et al. 2016) for velocity-aided attitude observer design. Hybrid nonlinear attitude and pose observers are proposed in (Berkane et al. 2017, Wang & Tayebi 2019) to overcome topological obstructions of Lie groups containing rotations (Bhat & Bernstein 2000) so that global asymptotical stability can be achieved. These are just a very non-exhaustive list of examples. On the other hand, other less explored research directions involve the Special Linear group SL(3) for homography estimation problem (Malis, Hamel, Mahony & Morin 2009, Mahony, Hamel, Morin & Malis 2012, Hamel, Mahony, Trumpf, Morin & Hua 2011, Hua, Hamel, Mahony & Allibert 2017, Hua, Trumpf, Hamel, Mahony & Morin 2019) and some newly introduced Lie groups for the Simultaneous Localization and Mapping (SLAM) problem such as the $\mathrm{SLAM}_n(3)$ group (Mahony & Hamel 2017), the $\mathrm{VSLAM}_n(3)$ group (van Goor, Mahony, Hamel & Trumpf 2019), and the $\mathrm{SE}_{n+1}(2)$ group (Barrau & Bonnabel 2015).

The present paper addresses the problem of nonlinear observer design on SL(3) with application to homography estimation and image stabilization. To our knowledge, most existing works on the topic have been proposed by the authors of this paper (Malis et al. 2009, Mahony et al. 2012, Hamel et al. 2011, Hua, Hamel, Mahony & Allibert 2017, Hua et al. 2019). Before providing further discussions, let us first recall on the homography and its importance in practice. Originated from the field of Computer Vision, the so-called homography is an invertible mapping that relates two camera views of the same planar scene by encoding in a single matrix the camera pose, the distance between the camera and the scene, along with the normal direction to the scene (e.g., (Hartley & Zisserman 2003)). It plays an important role in numerous computer vision and robotic applications where the scenarios involve man-made environments composed of (near) planar surfaces. The homography has been exploited to estimate the rigid-body pose of a robot equipped with a camera (Scaramuzza & Siegwart 2008). The navigation of robotic vehicles has been developed using homography sequences (de Plinval, Morin & Mouyon 2017) and one of the most successful visual servo control paradigms makes use of homographies (Malis, Chaumette & Boudet 1999). Homography-based navigation methods are also particularly well suited to applications where the camera is sufficiently far from the observed scene, such as situations where ground images are taken from an aerial vehicle (Caballero, Merino, Ferruz & Ollero 2007, de Plinval et al. 2017).

Let us now discuss about the homography estimation problem. Classical algorithms for homography estimation taken from the computer vision community consist in computing the homography on a frame-by-frame basis by solving algebraic constraints related to correspondences of image features (points, lines, conics, contours, etc.) (Hartley & Zisserman 2003, Agarwal, Jawahar & Narayanan 2005, Jain 2006, Kaminski & Shashua 2004, Conomis 2006). These algorithms, however, only consider the homography as an incidental variable and are not focused on improving (or filtering) the homography over time. This yields an obvious interest in developing alternative homography estimation algorithms that exploit the temporal correlation of data across a video sequence rather than computing algebraically individual raw homography for each image. Nonlinear observers provide a relevant answer to that preoccupation. In recent work by the co-authors of this paper (Mahony et al. 2012), a nonlinear observer has been proposed based on the underlying structure of the Special Linear group SL(3), which is isomorphic to the group of homographies (Benhimane & Malis 2007). Velocity information is exploited to interpolate across a sequence of images and improve the individual homography estimates. That observer, however, still requires

individual image homographies (previously computed using an algebraic technique) as feedback information. It thus necessitates both a classical homography algorithm and a temporal filter algorithm, and only functions if each pair of images provides sufficient features to algebraically compute a raw homography. In order to overcome these drawbacks, in our prior work (Hamel et al. 2011, Hua et al. 2019) the question of deriving an observer for a sequence of image homographies that takes image point-feature correspondences directly as input has been considered. In this paper, the previous observer is extended by also incorporating image line-feature correspondences (in addition to point-feature correspondences) directly as input in the design of observer innovation. In line with this effort, in another work (Hua, Hamel, Mahony & Allibert 2017) of the co-authors of this paper, conic-feature correspondences are considered for the construction of observer innovation, but the association of all these 3 types of features (i.e. points, lines, and conics) in direct observer design will require a careful investigation and is thus out of the scope of the present paper.

In this paper the proposed observer is derived based on an advanced theory for nonlinear observer design directly on the homogeneous output space (Mahony et al. 2013). Sharing the same filtering advantage with the observer in (Mahony et al. 2012), the advanced feature of both the observer of (Hamel et al. 2011, Hua et al. 2019) and the observer of this paper is the formulation of observer innovation that exploits directly point and line correspondences without requiring reconstruction of individual image homographies. This may save considerable computational resources, making the proposed algorithm suitable for embedded systems with simple feature tracking software. In contrast with algebraic techniques, the proposed algorithm is well posed even when there is insufficient data for full reconstruction of a homography. In such situations, the proposed observer continues to operate by incorporating available information and relying on propagation of prior estimates. Beyond the above practical advantages of the proposed observer, we believe that the present work is the first to address the problem of nonlinear observer design on the Special Linear group SL(3) for homography estimation by directly exploiting both point and line correspondences as input. It thereby constitutes an appealing application to the "school" of nonlinear observer design on Lie groups. Finally, technical rigourousness of the proposed observer is supported by comprehensive observability and stability analysis, which is also accompanied by a non-trivial analysis for a particular unobservable case often overlooked in the literature.

The present paper is organized as follows. Section 2 provides technical background. In Section 3 a nonlinear observer on SL(3) is proposed using direct point and line correspondences and the knowledge of the group velocity. In Section 4 the homography and associated homography velocity are related to rigid-body motion of the camera and two observers are derived for the case where only the angular velocity of the camera is known, a typical scenario in robotic applications. In Section 5, as a complement contribution, an application of the proposed approach to a real world problem in image stabilization is presented. Some video links, showing the experiment results, are provided as supplementary material. A preliminary version of this paper was reported in a technical report (Hua, Trumpf, Hamel, Mahony & Morin 2017).

2 Technical background

2.1 Notation and mathematical identities

- The Special Linear group SL(3) and its algebra $\mathfrak{sl}(3)$ are given by $\mathrm{SL}(3) := \{H \in \mathbb{R}^{3\times 3} \mid \det H = 1\}$ and $\mathfrak{sl}(3) := \{U \in \mathbb{R}^{3\times 3} \mid \mathrm{tr}(U) = 0\}$. The adjoint operator $\mathrm{Ad} : \mathrm{SL}(3) \times \mathfrak{sl}(3) \to \mathfrak{sl}(3)$ is defined by $\mathrm{Ad}_H U := HUH^{-1}$, $\forall H \in \mathrm{SL}(3)$, $U \in \mathfrak{sl}(3)$.
- Let $\langle \cdot, \cdot \rangle : \mathfrak{sl}(3) \times \mathfrak{sl}(3) \longrightarrow \mathbb{R}$ be an inner product on $\mathfrak{sl}(3)$, chosen to be the Euclidean matrix inner product on $\mathbb{R}^{3\times 3}$. Then, a right-invariant Riemannian metric on SL(3) induced by the inner product $\langle \cdot, \cdot \rangle$ is defined by $\langle U_1 H, U_2 H \rangle_H := \langle U_1, U_2 \rangle$, $\forall H \in \mathrm{SL}(3), U_1, U_2 \in \mathfrak{sl}(3)$.
- $\mathrm{grad}_1 f$ and $\mathrm{Hess}_1 f$ denote the gradient and Hessian in the first variable of f, respectively.
- $\{e_1, e_2, e_3\}$ denote the canonical basis of $\mathbb{R}^3$.
- $[\cdot]_\times$ is the skew-symmetric matrix associated with the vector cross-product, i.e. $[x]_\times y = x \times y$, $\forall x, y \in \mathbb{R}^3$.

2.2 Preliminaries about homographies

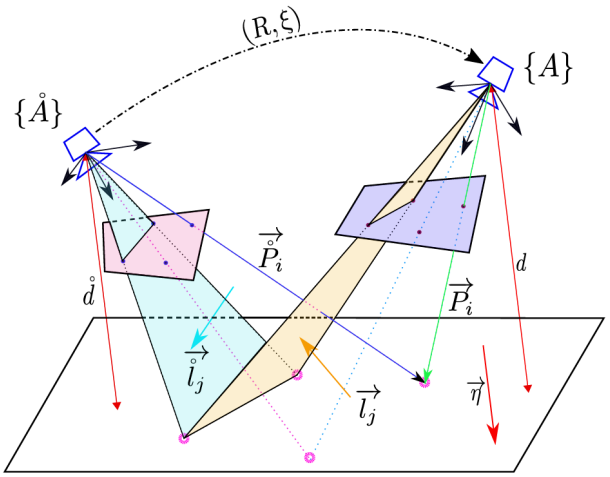

Fig. 1. The pose of the camera (R, ξ) determines a rigid body transformation from $\{A\}$ to $\{\mathring{A}\}$. The Euclidean homography $H :\cong R + (1/d)\xi\eta^\top$ maps Euclidean coordinates of the scene's points from $\{A\}$ to $\{\mathring{A}\}$. Arrow notation $(\vec{\cdot})$ is used for Euclidean vectors.

Let $\mathring{\mathcal{A}}$ (resp. $\mathcal{A}$) denote projective coordinates for the image plane of a camera $\mathring{A}$ (resp. A), and let $\{\mathring{A}\}$ (resp. $\{A\}$) denote its reference (resp. current) frame.

Let $\xi \in \mathbb{R}^3$ denote the position of the frame $\{A\}$ with respect to $\{\mathring{A}\}$ expressed in $\{\mathring{A}\}$. The orientation of the frame $\{A\}$ with respect to $\{\mathring{A}\}$ is represented by a rotation matrix $R \in \mathrm{SO}(3)$ (see Fig. 1).

Let us denote by $\mathring{d}$ (resp. d) and $\mathring{\eta}$ (resp. η) respectively the distance from the origin of $\{\mathring{A}\}$ (resp. $\{A\}$) to the observed planar scene and the normal vector pointing towards the scene expressed in $\{\mathring{A}\}$ (resp. $\{A\}$). One verifies that $\eta = R^\top \mathring{\eta}$ and $d = \mathring{d} - \mathring{\eta}^\top \xi$.

From the relation $\vec{\mathring{P}}_i = \vec{P}_i + \vec{\xi}$, the coordinates $\mathring{P}_i \in \{\mathring{A}\}$ and $P_i \in \{A\}$ of the same point of index $i \in \{1, \cdots, n\}$ on the scene are related by

$$\mathring{P}_i = RP_i + \xi. \tag{1}$$

Since the considered points belong to the observed planar scene $\Pi := \{P_i \in \mathbb{R}^3 : \eta^\top P_i - d = 0\}$, one deduces from the plane constraint $\frac{\eta^\top P_i}{d} = 1$ and Eq. (1) that

$$\mathring{P}_i = \left(R + \frac{\xi \eta^\top}{d}\right) P_i. \tag{2}$$

Let $\mathring{p}_i^{\mathrm{im}} \in \mathring{\mathcal{A}}$ (resp. $p_i^{\mathrm{im}} \in \mathcal{A}$) denote the image of the considered point of index i when the camera is aligned with the frame $\{\mathring{A}\}$ (resp. frame $\{A\}$) [2]. Note that $\mathring{p}_i^{\mathrm{im}}$ and p_i^{im} have the form $(u, v, 1)^\top$ using the homogeneous coordinate representation and they are related to the 3D coordinates of that point by [3]:

$$\mathring{p}_i^{\mathrm{im}} \cong K\mathring{P}_i, \quad p_i^{\mathrm{im}} \cong KP_i, \tag{3}$$

with $K \in \mathbb{R}^{3\times 3}$ the camera calibration matrix that contains the intrinsic parameters of the camera such as the focal length, the pixel aspect ratio, the principal point, etc (Ma et al. 2003). Assume that the camera is well calibrated (i.e. K is known) so that all quantities can be appropriately re-normalized onto the unit sphere $\mathbb{S}^2$ as

$$\mathring{p}_i := \frac{\mathring{P}_i}{|\mathring{P}_i|} = \frac{K^{-1}\mathring{p}_i^{\mathrm{im}}}{|K^{-1}\mathring{p}_i^{\mathrm{im}}|},\ p_i := \frac{P_i}{|P_i|} = \frac{K^{-1}p_i^{\mathrm{im}}}{|K^{-1}p_i^{\mathrm{im}}|}. \tag{4}$$

Using (2) and (4) the projected points satisfy

$$\mathring{p}_i \cong \left(R + \frac{\xi\eta^\top}{d}\right) p_i \cong Hp_i \ \Rightarrow\ p_i = \frac{H^{-1}\mathring{p}_i}{|H^{-1}\mathring{p}_i|}, \tag{5}$$

where the projective mapping $H : \mathcal{A} \to \mathring{\mathcal{A}}$, $H := R + \frac{\xi\eta^\top}{d}$ is the Euclidean homography that maps Euclidean coordinates of the scene's points from $\{A\}$ to $\{\mathring{A}\}$.

[2] The superscript $^{\mathrm{im}}$ is used for "image".

[3] Most statements in projective geometry involve equality up to a multiplicative constant denoted by $\cong$ or $\sim$ (Ma, Soatto, Kosecka & Sastry 2003). Relation (3) implies a well-known fact of monocular vision that the 3D coordinates of any observed point can only be retrieved from its corresponding image coordinates *up to a scale factor*.

Since a homography matrix H is only defined up to a scale factor, any homography matrix is associated with a unique matrix $\bar{H} \in \mathrm{SL}(3)$ by re-scaling $\bar{H} = \det(H)^{-\frac{1}{3}} H$ such that $\det(\bar{H}) = 1$. Therefore, without loss of generality it is assumed that H is an element of $\mathrm{SL}(3)$. Recall that the scale factor γ such that $H = \gamma\left(R + \frac{\xi\eta^\top}{d}\right)$ is equal $(d/\mathring{d})^{\frac{1}{3}}$ and corresponds to the second singular value of H (Ma et al. 2003). The so-called "image" homography matrix $G \in \mathrm{SL}(3)$ that maps pixel coordinates from $\mathcal{A}$ to $\mathring{\mathcal{A}}$ (i.e. $\mathring{p}_i^{\mathrm{im}} \cong Gp_i^{\mathrm{im}}$) then satisfies $G = KHK^{-1}$.

Any line on the observed scene can be represented by the unit vector $\vec{l}$ normal to the plane that contains the given line and the camera focal point. Picking arbitrarily two different points on the line of index $j \in \{1, \cdots, m\}$, one obtains

$$l_j = \frac{p_{1j} \times p_{2j}}{|p_{1j} \times p_{2j}|} \in \{A\},\ \mathring{l}_j = \frac{\mathring{p}_{1j} \times \mathring{p}_{2j}}{|\mathring{p}_{1j} \times \mathring{p}_{2j}|} \in \{\mathring{A}\}.$$

Using (5) and the property $M(a \times b) = \det(M)(M^{-\top}a \times M^{-\top}b)$ for any invertible matrix $M \in \mathbb{R}^{3\times 3}$ and $a, b \in \mathbb{R}^3$ one then deduces

$$l_j = \frac{H^{-1}\mathring{p}_{1j} \times H^{-1}\mathring{p}_{2j}}{|H^{-1}\mathring{p}_{1j} \times H^{-1}\mathring{p}_{2j}|} = \frac{H^\top(\mathring{p}_{1j} \times \mathring{p}_{2j})}{|H^\top(\mathring{p}_{1j} \times \mathring{p}_{2j})|} = \frac{H^\top \mathring{l}_j}{|H^\top \mathring{l}_j|}. \tag{6}$$

In the sequel, expressions (5) and (6) of point and line correspondences will be used as measurements for homography observer design.

3 Basic ideas of observer design on SL(3) based on direct point and line correspondences

3.1 Homography kinematics and measurements

To expose the underlying ideas of observer design, in this section we consider the simplified case where the kinematics of $H \in \mathrm{SL}(3)$ are given by

$$\dot{H} = F(H, U) := HU, \quad H(0) \in \mathrm{SL}(3), \tag{7}$$

with known group velocity $U \in \mathfrak{sl}(3)$. Section 4 will deal with a more applicative (and realistic) case where U is only partly measured.

Assume that a set of n (≥ 0) point measurements $p_i \in \mathbb{S}^2$ and/or a set of m (≥ 0) line measurements $l_j \in \mathbb{S}^2$ are at our disposal. All these measurements are expressed in the camera current frame $\{A\}$:

$$p_i = h_p(H, \mathring{p}_i) := \frac{H^{-1}\mathring{p}_i}{|H^{-1}\mathring{p}_i|}, \quad i = \{1, \ldots, n\}, \tag{8}$$

$$l_j = h_l(H, \mathring{l}_j) := \frac{H^\top \mathring{l}_j}{|H^\top \mathring{l}_j|}, \quad j = \{1, \ldots, m\}, \tag{9}$$

where $\mathring{p}_i \in \mathbb{S}^2$ and $\mathring{l}_j \in \mathbb{S}^2$ are constant and known in the reference frame $\{\mathring{A}\}$. For future reference, define

$$\mathring{p} := (\mathring{p}_1, \cdots, \mathring{p}_n),\ p := (p_1, \cdots, p_n),$$
$$\mathring{l} := (\mathring{l}_1, \cdots, \mathring{l}_m),\ l := (l_1, \cdots, l_m).$$

For stability analysis purposes, the following observability assumption is introduced and will be discussed thereafter.

Assumption 1 (Observability conditions) *Assume that the union set $\mathcal{S} := \mathcal{S}_p^n \bigcup \mathcal{S}_l^m$, with $\mathcal{S}_p^n$ the set of $n\ (\geq 0)$ observed constant points $\mathring{p}_i \in \mathbb{S}^2$ and $\mathcal{S}_l^m$ the set of $m\ (\geq 0)$ observed constant lines $\mathring{l}_j \in \mathbb{S}^2$, is* ***consistent*** *in the sense that $\mathcal{S}$ satisfies one of the four following cases*[4] *:*

- ***Case 1 (at least 4 points):*** *There exists a subset $\mathcal{S}_p^4 \subset \mathcal{S}_p^n$ of 4 points such that all vector triplets in $\mathcal{S}_p^4$ are linearly independent.*
- ***Case 2 (at least 4 lines):*** *There exists a subset $\mathcal{S}_l^4 \subset \mathcal{S}_l^n$ of 4 lines such that all vector triplets in $\mathcal{S}_l^4$ are linearly independent.*
- ***Case 3 (at least 3 points and 1 line):*** *There exist 1 line $\mathring{l}_j$ and a subset $\mathcal{S}_p^3 \subset \mathcal{S}_p^n$ of 3 linearly independent points that do not lie on the line $\mathring{l}_j$, i.e. $\mathring{l}_j^\top \mathring{p}_i \neq 0$, $\forall \mathring{p}_i \in \mathcal{S}_p^3$.*
- ***Case 4 (at least 1 point and 3 lines):*** *There exist a subset $\mathcal{S}_l^3 \subset \mathcal{S}_l^m$ of 3 linearly independent lines and 1 point $\mathring{p}_i$ that does not lie on any line of $\mathcal{S}_l^3$, i.e. $\mathring{l}_j^\top \mathring{p}_i \neq 0$, $\forall \mathring{l}_j \in \mathcal{S}_l^3$.*

One verifies that SL(3) is a symmetry group with group actions

$$\begin{aligned}
\phi(Q,H) &:= HQ,\\
\psi(Q,U) &:= Ad_{Q^{-1}}U = Q^{-1}UQ,\\
\rho(Q,p) &:= \frac{Q^{-1}p}{|Q^{-1}p|},\\
\mu(Q,l) &:= \frac{Q^\top l}{|Q^\top l|},
\end{aligned}$$

which are *right group actions* in the sense that $\phi(Q_2, \phi(Q_1, H)) = \phi(Q_1Q_2, H)$, $\psi(Q_2, \psi(Q_1, U)) = \psi(Q_1Q_2,\ U)$, $\rho(Q_2,\ \rho(Q_1,\ p)) = \rho(Q_1Q_2,\ p)$, and $\mu(Q_2, \mu(Q_1, p)) = \mu(Q_1Q_2, p)$ whatever $Q_1, Q_2, H \in \mathrm{SL}(3)$, $U \in \mathfrak{sl}(3)$, and $p, l \in \mathbb{S}^2$.

The kinematics are *right equivariant* since it can be verified that

$$\begin{cases}
d_H\phi(Q,H)[F(H,U)] = F(\phi(Q,H), \psi(Q,U))\\
\rho(Q, h_p(H, \mathring{p}_i)) \quad\ = h_p(\phi(Q,H), \mathring{p}_i)\\
\mu(Q, h_l(H, \mathring{l}_i)) \quad\ = h_l(\phi(Q,H), \mathring{l}_i)
\end{cases}$$

which have the same forms as the system equation (7) and the output equations (8), (9). The fact that the kinematics are right equivariant allows for applying the nonlinear observer design framework developed in (Mahony et al. 2013).

3.2 Equivariant observer design on SL(3) based on point and line correspondences

Let $\hat{H} \in \mathrm{SL}(3)$ denote the estimate of H. Define the right group error $E := \hat{H}H^{-1} \in \mathrm{SL}(3)$ and the output errors $e_{pi} \in \mathbb{S}^2$, with $i \in \{1, \cdots, n\}$, and $e_{lj} \in \mathbb{S}^2$, with $j \in \{1, \cdots, m\}$, as:

$$e_{pi} := \rho(\hat{H}^{-1}, p_i) = \frac{\hat{H}p_i}{|\hat{H}p_i|} = \frac{E\mathring{p}_i}{|E\mathring{p}_i|}, \tag{10}$$

$$e_{lj} := \mu(\hat{H}^{-1}, l_j) = \frac{\hat{H}^{-\top}l_j}{|\hat{H}^{-\top}l_j|} = \frac{E^{-\top}\mathring{l}_j}{|E^{-\top}\mathring{l}_j|}. \tag{11}$$

The general form of the proposed observer is given by

$$\dot{\hat{H}} = \hat{H}U - \Delta(\hat{H}, p, l)\hat{H}, \quad \hat{H}(0) \in \mathrm{SL}(3) \tag{12}$$

with $\Delta(\hat{H}, p, l) \in \mathfrak{sl}(3)$ the innovation term to be designed.
According to (Mahony et al. 2013, Th. 1), if the innovation term $\Delta(\hat{H}, p, l)$ is *right equivariant* in the sense that

$$\begin{aligned}
&\Delta(\phi(Q,\hat{H}), \rho(Q,p_1), \cdots, \rho(Q,p_n), \mu(Q,l_1), \cdots, \mu(Q,l_m))\\
&= \Delta(\hat{H}, p_1, \cdots, p_n, l_1, \cdots, l_m), \quad \forall Q \in \mathrm{SL}(3),
\end{aligned}$$

then the dynamics of the group error E are autonomous:

$$\dot{E} = -\Delta(E, \mathring{p}, \mathring{l})E. \tag{13}$$

To determine the right-equivariant innovation $\Delta(\hat{H}, p, l)$, a *right-invariant* cost function $\mathcal{C}(\hat{H}, p, l)$ should be defined. To this purpose, we first define individual right-invariant cost functions at $\mathring{p}_i$ or $\mathring{l}_j$ on the output space $\mathbb{S}^2$ as follows:

$$\begin{aligned}
\mathcal{C}_{\mathring{p}_i}(\hat{H}, p_i) &:= \tfrac{k_i}{2}\left|\tfrac{\hat{H}p_i}{|\hat{H}p_i|} - \mathring{p}_i\right|^2,\\
\mathcal{C}_{\mathring{l}_j}(\hat{H}, l_j) &:= \tfrac{\kappa_j}{2}\left|\tfrac{\hat{H}^{-\top}l_j}{|\hat{H}^{-\top}l_j|} - \mathring{l}_j\right|^2,
\end{aligned}$$

with $k_i, \kappa_j > 0$. These cost functions are right invariant since $\mathcal{C}_{\mathring{p}_i}(\phi(Q,\hat{H}), \rho(Q,p_i)) = \mathcal{C}_{\mathring{p}_i}(\hat{H}, p_i)$ and $\mathcal{C}_{\mathring{l}_j}(\phi(Q,\hat{H}), \mu(Q,p_i)) = \mathcal{C}_{\mathring{l}_j}(\hat{H}, l_j)$, $\forall Q \in \mathrm{SL}(3)$. Then, the aggregate cost $\mathcal{C}(\hat{H}, p, l)$ defined as the sum of all the individual cost functions

$$\mathcal{C}(\hat{H}, p, l) := \sum_{i=1}^{n} \frac{k_i}{2}\left|\frac{\hat{H}p_i}{|\hat{H}p_i|} - \mathring{p}_i\right|^2 + \sum_{j=1}^{m} \frac{\kappa_j}{2}\left|\frac{\hat{H}^{-\top}l_j}{|\hat{H}^{-\top}l_j|} - \mathring{l}_j\right|^2 \tag{14}$$

is also right invariant.

[4] The homography for case of 2 points and 2 lines is not observable and cannot be algebraically reconstructed (Hartley & Zisserman 2003).

From there the innovation term $\Delta(\hat{H},p,l)$ can be computed as (Mahony et al. 2013, Eq. (40))

$$\Delta(\hat{H},p,l) = (\mathrm{grad}_1\mathcal{C}(\hat{H},p,l))\hat{H}^{-1}, \tag{15}$$

with grad_1 the gradient using a *right-invariant Riemannian metric* on SL(3).

Using the fact that the considered Riemannian metric is right invariant, one obtains

$$\begin{aligned} d_{\hat{H}}\mathcal{C}(\hat{H},p,l)[U\hat{H}] &= \langle \mathrm{grad}_1\mathcal{C}(\hat{H},p,l), U\hat{H}\rangle_H \\ &= \langle \mathrm{grad}_1\mathcal{C}(\hat{H},p,l)\hat{H}^{-1}\hat{H}, U\hat{H}\rangle_H \\ &= \langle \mathrm{grad}_1\mathcal{C}(\hat{H},p,l)\hat{H}^{-1}, U\rangle \\ &= \langle \Delta(\hat{H},p,l), U\rangle, \end{aligned} \tag{16}$$

with any $U \in \mathfrak{sl}(3)$. On the other hand, using (14) one has

$$\begin{aligned} &d_{\hat{H}}\mathcal{C}(\hat{H},p,l)[U\hat{H}] \\ &= \textstyle\sum_{i=1}^n k_i \left(\frac{\hat{H}p_i}{|\hat{H}p_i|} - \mathring{p}_i\right)^\top \left(I - \frac{(\hat{H}p_i)(\hat{H}p_i)^\top}{|\hat{H}p_i|^2}\right)\frac{(U\hat{H})p_i}{|\hat{H}p_i|} \\ &+ \textstyle\sum_{j=1}^m \kappa_j \left(\frac{\hat{H}^{-\top}l_j}{|\hat{H}^{-\top}l_j|} - \mathring{l}_j\right)^\top \left(I - \frac{(\hat{H}^{-\top}l_j)(\hat{H}^{-\top}l_j)^\top}{|\hat{H}^{-\top}l_j|^2}\right)\frac{(-U^\top\hat{H}^{-\top})l_j}{|\hat{H}^{-\top}l_j|} \\ &= \textstyle\sum_{i=1}^n k_i (e_{pi} - \mathring{p}_i)^\top (I - e_{pi}e_{pi}^\top)Ue_{pi} \\ &- \textstyle\sum_{j=1}^m \kappa_i (e_{lj} - \mathring{l}_j)^\top (I - e_{lj}e_{lj}^\top)U^\top e_{lj} \\ &= -\mathrm{tr}\left(\textstyle\sum_{i=1}^n k_i \pi_{e_{pi}}\mathring{p}_i e_{pi}^\top U^\top\right) + \mathrm{tr}\left(\textstyle\sum_{j=1}^m \kappa_j e_{lj}\mathring{l}_j^\top \pi_{e_{lj}}U^\top\right) \\ &= \left\langle -\textstyle\sum_{i=1}^n k_i \pi_{e_{pi}}\mathring{p}_i e_{pi}^\top + \sum_{j=1}^m \kappa_j e_{lj}\mathring{l}_j^\top \pi_{e_{lj}}, U\right\rangle, \end{aligned} \tag{17}$$

with $\pi_x := (I - xx^\top)$, $\forall x \in \mathbb{S}^2$. One directly deduces from (16) and (17) the expression of the innovation term $\Delta(\hat{H},p,l)$ as

$$\Delta(\hat{H},p,l) = -\sum_{i=1}^n k_i \pi_{e_{pi}}\mathring{p}_i e_{pi}^\top + \sum_{j=1}^m \kappa_j e_{lj}\mathring{l}_j^\top \pi_{e_{lj}}. \tag{18}$$

One deduces from (18) that $\Delta(E,\mathring{p},\mathring{l}) = \Delta(\hat{H},p,l)$ and, consequently, from (13) that

$$\dot{E} = \Big(\sum_{i=1}^n k_i \pi_{e_{pi}}\mathring{p}_i e_{pi}^\top - \sum_{j=1}^m \kappa_j e_{lj}\mathring{l}_j^\top \pi_{e_{lj}}\Big)E. \tag{19}$$

Theorem 1 *Consider the kinematics* (7) *and assume that the group velocity* $U \in \mathfrak{sl}(3)$ *is known. Consider Observer* (12) *with the innovation term* $\Delta(\hat{H},p,l) \in \mathfrak{sl}(3)$ *defined by* (18)*. Assume that Assumption 1 holds. Then, the equilibrium* $E = I$ *of the error system* (19) *is locally exponentially stable.*

Proof: The proof of this theorem is based on Theorem 2 in (Mahony et al. 2013) according to which the equilibrium $E = I$ of system (19) is locally exponentially stable if the right-invariant cost function $\mathcal{C}(\hat{H},p,l)$ defined by (14) is *non-degenerate* (i.e. $(I,\mathring{p},\mathring{l})$ is a global minimum of $\mathcal{C}(\hat{H},p,l)$). According to (Mahony et al. 2013, Lem. 3), $\mathcal{C}(\hat{H},p,l)$ is non-degenerate if

$$\big(\textstyle\bigcap_{i=1}^n \mathrm{stab}_\rho(\mathring{p}_i)\big) \bigcap \big(\bigcap_{j=1}^m \mathrm{stab}_\mu(\mathring{l}_j)\big) = \{I\}, \tag{20}$$

where the stabilizer $\mathrm{stab}_f(y)$ (here f stands for either ρ or μ) of an element $y \in \mathbb{S}^2$ is defined by

$$\mathrm{stab}_f(y) := \big\{Q \in \mathrm{SL}(3) \mid f(Q,y) = y\big\}.$$

Condition (20) is, in fact, equivalent to

$$\mathfrak{s} := \big(\textstyle\bigcap_{i=1}^n \mathfrak{s}_{\rho i}\big) \bigcap \big(\bigcap_{j=1}^m \mathfrak{s}_{\mu j}\big) = \{0\}, \tag{21}$$

with

$$\begin{aligned} \mathfrak{s}_{\rho i} &:= \ker(\mathrm{d}_H\rho(H,\mathring{p}_i)|_{H=I}), \\ \mathfrak{s}_{\mu j} &:= \ker(\mathrm{d}_H\mu(H,\mathring{l}_j)|_{H=I}), \end{aligned}$$

the Lie-algebra associated with $\mathrm{stab}_\rho(\mathring{p}_i)$ and $\mathrm{stab}_\mu(\mathring{l}_j)$, respectively. In fact, condition (20) or, equivalently, (21) ensures that the Hessian $\mathrm{Hess}_1\mathcal{C}(I,\mathring{p},\mathring{l})$ is positive definite (Mahony et al. 2013).

Therefore, the remainder of the proof consists in proving that condition (21) is satisfied subject to Assumption 1. To this purpose, one first computes the derivatives

$$\begin{aligned} \mathrm{d}_H\rho(H,\mathring{p}_i)[HU] &= \mathrm{d}\left(\frac{H^{-1}\mathring{p}_i}{|H^{-1}\mathring{p}_i|}\right)[HU] \\ &= -\left(I - \frac{(H^{-1}\mathring{p}_i)(H^{-1}\mathring{p}_i)^\top}{|H^{-1}\mathring{p}_i|^2}\right)\frac{UH^{-1}\mathring{p}_i}{|H^{-1}\mathring{p}_i|}, \end{aligned}$$

$$\begin{aligned} \mathrm{d}_H\mu(H,\mathring{l}_j)[HU] &= \mathrm{d}\left(\frac{H^\top\mathring{l}_j}{|H^\top\mathring{l}_j|}\right)[HU] \\ &= \left(I - \frac{(H^\top\mathring{l}_j)(H^\top\mathring{l}_j)^\top}{|H^\top\mathring{l}_j|^2}\right)\frac{U^\top H^\top\mathring{l}_j}{|H^{-1}\mathring{l}_j|}, \end{aligned}$$

with any $U \in \mathfrak{sl}(3)$. From there one deduces

$$\mathfrak{s}_{\rho i} = \ker(\mathrm{d}_H\rho(H,\mathring{p}_i)|_{H=I}) = \{U \in \mathfrak{sl}(3) \mid \pi_{\mathring{p}_i}U\mathring{p}_i = 0\},$$

$$\mathfrak{s}_{\mu j} = \ker(\mathrm{d}_H\mu(H,\mathring{l}_j)|_{H=I}) = \{U \in \mathfrak{sl}(3) \mid \pi_{\mathring{l}_j}U^\top\mathring{l}_j = 0\},$$

and, subsequently,

$$\begin{aligned} &\mathfrak{s} = (\textstyle\bigcap_{i=1}^n \mathfrak{s}_{\rho i}) \bigcap (\bigcap_{j=1}^m \mathfrak{s}_{\mu j}) = \\ &\big\{U \in \mathfrak{sl}(3) \,|\, \pi_{\mathring{p}_i}U\mathring{p}_i = 0, \pi_{\mathring{l}_j}U^\top\mathring{l}_j = 0, \forall \mathring{p}_i \in \mathcal{S}_p^n,\, \mathring{l}_j \in \mathcal{S}_l^m\big\}. \end{aligned} \tag{22}$$

We will determine $U \in \mathfrak{sl}(3)$ such that $\pi_{\mathring{p}_i}U\mathring{p}_i = 0$ and $\pi_{\mathring{l}_j}U^\top\mathring{l}_j = 0$, for all $i = 1,\cdots,n$ and $j = 1,\cdots,m$. The relations $\pi_{\mathring{p}_i}U\mathring{p}_i = 0$ and $\pi_{\mathring{l}_j}U^\top\mathring{l}_j = 0$ can be equivalently written as $U\mathring{p}_i = \lambda_{pi}\mathring{p}_i$ and $U^\top\mathring{l}_j = \lambda_{lj}\mathring{l}_j$, with $\lambda_{pi} := \mathring{p}_i^\top U\mathring{p}_i$ and $\lambda_{lj} := \mathring{l}_j^\top U\mathring{l}_j$. From there one deduces that λ_{pi} (resp. λ_{lj}) are eigenvalues of U (resp. $U^\top$) and $\mathring{p}_i$ (resp. $\mathring{l}_j$) are the associated eigenvectors. Consider the 4 cases of Assumption 1.

• ***Case 1 (at least*** 4 ***points):*** Without loss of generality, assume that the subset $\mathcal{S}_p^4 = \{\mathring{p}_1, \mathring{p}_2, \mathring{p}_3, \mathring{p}_4\}$ is consistent. Thus, there exist 3 non-zero numbers b_1, b_2, and b_3 such that $\mathring{p}_4 = \sum_{i=1}^3 b_i \mathring{p}_i$. From there using the fact that

$$U\mathring{p}_4 = U\sum_{i=1}^3 b_i\mathring{p}_i = \sum_{i=1}^3 b_i U\mathring{p}_i = \sum_{i=1}^3 b_i\lambda_{pi}\mathring{p}_i,$$

$$U\mathring{p}_4 = \lambda_{p4}\mathring{p}_4 = \lambda_{p4}\sum_{i=1}^3 b_i\mathring{p}_i = \sum_{i=1}^3 b_i\lambda_{p4}\mathring{p}_i,$$

one deduces

$$\sum_{i=1}^3 b_i\lambda_{pi}\mathring{p}_i = \sum_{i=1}^3 b_i\lambda_{p4}\mathring{p}_i. \tag{23}$$

Since b_i $(i = 1, 2, 3)$ are not null and the 3 unit vectors $\mathring{p}_i$ $(i = 1, 2, 3)$ are linearly independent, (23) directly yields $\lambda_{p1} = \lambda_{p2} = \lambda_{p3} = \lambda_{p4}$. Let λ denote the value of these identical eigenvalues. One deduces that U has a triple eigenvalue λ. Since the number of linearly independent eigenvectors of U is equal to 3, the matrix U is diagonalizable. Then, the diagonalizability of U along with the fact that it has a triple eigenvalue implies that $U = \lambda I$. This in turn yields $\mathrm{tr}(U) = 3\lambda$, which is zero since U is an element of $\mathfrak{sl}(3)$. Consequently, $\lambda = 0$ and $U = 0$. One then deduces $\mathfrak{s} = \{0\}$.

• ***Case 2 (at least*** 4 ***lines):*** By proceeding analogously to the proof for Case 1, one deduces that $U^\top$ has a triple eigenvalue λ and $U^\top = \lambda I$. Since $\mathrm{tr}(U^\top) = 0$, one deduces $\lambda = 0$, $U = 0$ and, consequently, $\mathfrak{s} = \{0\}$.

• ***Case 3 (at least*** 3 ***points and*** 1 ***line):*** Without loss of generality, assume that the subset $\mathcal{S}_p^3 = \{\mathring{p}_1, \mathring{p}_2, \mathring{p}_3\}$ contains 3 linearly independent points that do not lie on the line $\mathring{l}_1$, i.e. $\mathring{l}_1^\top\mathring{p}_i \neq 0, \forall \mathring{p}_i \in \mathcal{S}_p^3$. Using the relations $U\mathring{p}_i = \lambda_{pi}\mathring{p}_i$, one obtains $\mathring{l}_1^\top(U\mathring{p}_i) = \lambda_{pi}\mathring{l}_1^\top\mathring{p}_i$. On the other hand, using the relation $U^\top\mathring{l}_1 = \lambda_{l1}\mathring{l}_1$, one has $\mathring{l}_1^\top(U\mathring{p}_i) = \mathring{p}_i^\top(U^\top\mathring{l}_1) = \lambda_{l1}\mathring{p}_i^\top\mathring{l}_1$. Consequently, one deduces $\lambda_{p1} = \lambda_{p2} = \lambda_{p3} = \lambda_{l1}$. This means that U has a triple eigenvalue associated with 3 linearly independent eigenvectors $\mathring{p}_{1,2,3}$. One then deduces that $U = 0$ and, consequently, $\mathfrak{s} = \{0\}$.

• ***Case 4 (at least*** 1 ***point and*** 3 ***lines):*** Without loss of generality, assume that the subset $\mathcal{S}_l^3 = \{\mathring{l}_1, \mathring{l}_2, \mathring{l}_3\}$ contains 3 linearly independent lines and that the point $\mathring{p}_1$ does not lie on any line of $\mathcal{S}_l^3$, i.e. $\mathring{l}_j^\top\mathring{p}_1 \neq 0, \forall \mathring{l}_j \in \mathcal{S}_l^3$. Then, by proceeding analogously to the proof for Case 3, one deduces that $\lambda_{l1} = \lambda_{l2} = \lambda_{l3} = \lambda_{p1}$, which means that $U^\top$ has a triple eigenvalue associated with 3 linearly independent eigenvectors $\mathring{l}_{1,2,3}$. One then deduces that $U = 0$ and, consequently, $\mathfrak{s} = \{0\}$ *(end of proof)*. ∎

Now some discussions on Assumption 1 are in order.

• The four cases of Assumption 1 correspond to the ones discussed by Hartley and Zisserman in (Hartley & Zisserman 2003, p. 93) where algebraic reconstruction of the homography is possible from the correspondences of mixed-type features, namely points and lines. Here instead of using geometric constraint arguments to fully cover the 8 degrees of freedom of the homography like in (Hartley & Zisserman 2003), we have followed a more "Automatic Control" approach so as to tackle (see the proof of Theorem 1) the observability conditions (given in Assumption 1) in a more explicit manner.

• Regarding the "unobservable" case with *2 point and 2 line correspondences* also discussed in (Hartley & Zisserman 2003, p. 93), it can be proved that this case does not ensure the satisfaction of the observability condition (20) (or equivalently (21)). In fact, similarly to the proof of Theorem 1 and in view of (22), it suffices to prove that there exists some non-null matrix $U \in \mathfrak{sl}(3)$ such that $\pi_{\mathring{p}_i}U\mathring{p}_i = 0$ and $\pi_{\mathring{l}_j}U^\top\mathring{l}_j = 0$, for all $i = 1, 2$ and $j = 1, 2$. Assume that the two considered points do not coincide (i.e. $\mathring{p}_1^\top\mathring{p}_2 \neq 1$) and do not lie on any of the two considered lines (i.e. $\mathring{p}_i^\top\mathring{l}_j \neq 0$, $\forall i, j \in \{1, 2\}$). Then by proceeding analogously to the proof for Cases 3 and 4 in Theorem 1, one deduces that $\lambda_{p_1} = \lambda_{p_2} = \lambda_{l_1} = \lambda_{l_2} = \lambda$ and, thus,

$$U\mathring{p}_1 = \lambda\mathring{p}_1,\ U\mathring{p}_2 = \lambda\mathring{p}_2,\ U^\top\mathring{l}_1 = \lambda\mathring{l}_1,\ U^\top\mathring{l}_2 = \lambda\mathring{l}_2. \tag{24}$$

In order to determine $U \in \mathfrak{sl}(3)$ solution to (24), let us first define $\alpha := \mathrm{acos}(\mathring{p}_1^\top\mathring{p}_2) \neq 0$. One then verifies that there exists a unique rotation matrix $R_p \in \mathrm{SO}(3)$ such that $R_p\mathring{p}_1 = e_3$ and $R_p\mathring{p}_2 = \sin\alpha\, e_1 + \cos\alpha\, e_3$. In fact, R_p can be easily determined using the TRIAD algorithm (Shuster 1978). Then, via the following change of variables:

$$\bar{U} := R_pUR_p^\top,\ \bar{\mathring{l}}_1 := R_p\mathring{l}_1,\ \bar{\mathring{l}}_2 := R_p\mathring{l}_2,$$

the equalities in (24) can be rewritten as

$$\begin{aligned}
&\bar{U}e_3 = \lambda e_3,\\
&\bar{U}(\sin\alpha\, e_1 + \cos\alpha\, e_3) = \lambda(\sin\alpha\, e_1 + \cos\alpha\, e_3),\\
&\bar{U}^\top\bar{\mathring{l}}_1 = \lambda\bar{\mathring{l}}_1,\ \bar{U}^\top\bar{\mathring{l}}_2 = \lambda\bar{\mathring{l}}_2,
\end{aligned}$$

from which, and using the fact that $\mathrm{tr}(\bar{U}) = \mathrm{tr}(U) = 0$ and $\sin\alpha \neq 0$, one easily deduces that $\bar{U} = \lambda\bar{U}_0$, with

$$\bar{U}_0 := \begin{bmatrix} 1 & \frac{3(\bar{\mathring{l}}_{12}\bar{\mathring{l}}_{23} - \bar{\mathring{l}}_{13}\bar{\mathring{l}}_{22})}{\bar{\mathring{l}}_{11}\bar{\mathring{l}}_{23} - \bar{\mathring{l}}_{13}\bar{\mathring{l}}_{21}} & 0 \\ 0 & -2 & 0 \\ 0 & \frac{3(\bar{\mathring{l}}_{12}\bar{\mathring{l}}_{21} - \bar{\mathring{l}}_{11}\bar{\mathring{l}}_{22})}{\bar{\mathring{l}}_{11}\bar{\mathring{l}}_{23} - \bar{\mathring{l}}_{13}\bar{\mathring{l}}_{21}} & 1 \end{bmatrix}$$

and, thus, $\mathfrak{s} = \{\lambda R_p^\top\bar{U}_0R_p, \forall\lambda \in \mathbb{R}\} \neq \{0\}$, meaning that (21) is not satisfied.

4 Application to camera-IMU systems observing a stationary planar scene

4.1 Homography kinematics from a camera moving with rigid-body motion

In this section the situation where a sequence of homographies is generated by a moving camera viewing a stationary planar scene (i.e. $\{\mathring{A}\}$ is stationary) is considered. The objective consists in developing a nonlinear

filter for the image homography sequence using the velocity associated with the rigid-body motion of the camera rather than the group velocity U as was assumed in Section 3.

The kinematics of the camera's pose (R, ξ) are given by

$$\begin{cases} \dot{R}=R[\Omega]_\times \\ \dot{\xi} =RV \end{cases} \tag{25}$$

with $\Omega \in \mathbb{R}^3$ and $V \in \mathbb{R}^3$ denoting the angular velocity and linear velocity of $\{A\}$ with respect to $\{\mathring{A}\}$ expressed in $\{A\}$, respectively.

The group velocity $U \in \mathfrak{sl}(3)$ induced by the rigid-body motion and involved in the dynamics (7) of H satisfies (Mahony et al. 2012)

$$U = [\Omega]_\times + \frac{V\eta^\top}{d} - \frac{\eta^\top V}{3d} I. \tag{26}$$

Note that the variables η and d involved in U are not measurable and cannot be extracted directly from the measurements. In the sequel, one rewrites (26) as

$$U = [\Omega]_\times + \Gamma = [\Omega]_\times + \Gamma_1 - \frac{1}{3}\mathrm{tr}(\Gamma_1) I, \tag{27}$$

with $\Gamma := \frac{V\eta^\top}{d} - \frac{\eta^\top V}{3d} I$ and $\Gamma_1 := \frac{V\eta^\top}{d}$.

Since $\{\mathring{A}\}$ is stationary by assumption, the angular velocity Ω can be directly measured from the set of embedded gyrometers. The term Γ related to the translational motion expressed in the current frame $\{A\}$ is more involved. If it is assumed that $\frac{\dot{\xi}}{d}$ is constant (e.g., the camera moving with a constant velocity parallel to the scene or converging exponentially towards it), and using the fact that $V = R^\top \dot{\xi}$ and $\dot{\eta} = \eta \times \Omega$, one verifies that

$$\dot{\Gamma} = [\Gamma, [\Omega]_\times], \tag{28}$$

with $[\Gamma, [\Omega]_\times] = \Gamma[\Omega]_\times - [\Omega]_\times \Gamma$ the Lie bracket.

On the other hand, if it is assumed that $\frac{V}{d}$ is constant (e.g., the camera following a circular trajectory over the scene or performing an exponential convergence towards it), it follows that

$$\dot{\Gamma}_1 = \Gamma_1 [\Omega]_\times. \tag{29}$$

4.2 Observer design with measured angular velocity of the rigid body

Consider the case where the part Γ (resp. Γ_1) of the group velocity U in (27) is not available to measurement. Let $\hat{\Gamma}$ (resp. $\hat{\Gamma}_1$) denote the estimate of Γ (resp. Γ_1) and define the error term

$$\tilde{\Gamma} := \Gamma - \hat{\Gamma}, \quad (\text{resp. } \tilde{\Gamma}_1 := \Gamma_1 - \hat{\Gamma}_1).$$

The goal is to provide an estimate $\hat{H} \in \mathrm{SL}(3)$ of H to drive the group error $E\,(= \hat{H}H^{-1})$ to the identity matrix I and the error term $\tilde{\Gamma}$ (resp. $\tilde{\Gamma}_1$) to 0 if Γ (resp. Γ_1) is assumed to be constant.

The observer when $\frac{\dot{\xi}}{d}$ is constant is proposed as follows (compare to (12)):

$$\begin{cases} \dot{\hat{H}} & = \hat{H}([\Omega]_\times + \hat{\Gamma}) - \Delta(\hat{H}, p, l)\hat{H} \\ \dot{\hat{\Gamma}} & = [\hat{\Gamma}, [\Omega]_\times] - k_I \mathrm{Ad}_{\hat{H}^\top} \Delta(\hat{H}, p, l) \\ \hat{H}(0) \in \mathrm{SL}(3), & \quad \hat{\Gamma}(0) \in \mathfrak{sl}(3) \end{cases} \tag{30}$$

and the observer when $\frac{V}{d}$ is constant is proposed as follows:

$$\begin{cases} \dot{\hat{H}} & = \hat{H}([\Omega]_\times + \hat{\Gamma}_1 - \frac{1}{3}\mathrm{tr}(\hat{\Gamma}_1) I) - \Delta(\hat{H}, p, l)\hat{H} \\ \dot{\hat{\Gamma}}_1 & = \hat{\Gamma}_1 [\Omega]_\times - k_I \mathrm{Ad}_{\hat{H}^\top} \Delta(\hat{H}, p, l) \\ \hat{H}(0) \in \mathrm{SL}(3), & \quad \hat{\Gamma}_1(0) \in \mathfrak{sl}(3) \end{cases} \tag{31}$$

with some positive gain k_I and $\Delta(\hat{H}, p, l)$ given by (18).

The following proposition establishes stability result for Observer (30). The same result for Observer (31) can be directly stated.

Proposition 1 *Consider a camera moving with kinematics* (25) *viewing a static planar scene. Assume that* Ω *is measured and bounded. Consider the kinematics* (7) *along with* (27)*. Assume that* H *is bounded and that* Γ *obeys* (28)*. Consider Observer* (30) *along with the innovation* $\Delta(\hat{H}, p, l) \in \mathfrak{sl}(3)$ *defined by* (18)*. Assume that Assumption 1 holds. Then, the equilibrium* $(E, \tilde{\Gamma}) = (I, 0)$ *of the error system is locally asymptotically stable.*

Proof: One verifies that the error dynamics satisfy

$$\begin{cases} \dot{E}=-(\Delta + \mathrm{Ad}_{\hat{H}} \tilde{\Gamma})E \\ \dot{\tilde{\Gamma}} = [\tilde{\Gamma}, [\Omega]_\times] + k_I \mathrm{Ad}_{\hat{H}^\top} \Delta \end{cases} \tag{32}$$

with Δ the shortened notation of $\Delta(\hat{H}, p, l)$. From (10), (11) and (32) one deduces

$$\begin{cases} \dot{e}_{p_i} = -\pi_{e_{p_i}} (\Delta + \mathrm{Ad}_{\hat{H}} \tilde{\Gamma}) e_{p_i} \\ \dot{e}_{l_j} = \pi_{e_{l_j}} (\Delta + \mathrm{Ad}_{\hat{H}} \tilde{\Gamma})^\top e_{l_j} \end{cases} \tag{33}$$

Consider the following Lyapunov function candidate:

$$\begin{aligned} \mathcal{L} &:= \sum_{i=1}^{n} \frac{k_i}{2} |e_{p_i} - \mathring{p}_i|^2 + \sum_{j=1}^{m} \frac{\kappa_j}{2} \left| e_{l_j} - \mathring{l}_j \right|^2 + \frac{1}{2k_I} ||\tilde{\Gamma}||^2 \\ &= \mathcal{C}(E, \mathring{p}, \mathring{l}) + \frac{1}{2k_I} ||\tilde{\Gamma}||^2. \end{aligned} \tag{34}$$

with $\mathcal{C}(\cdot, \cdot, \cdot)$ defined by (14) (Note that $\mathcal{C}(\hat{H}, p, l) = \mathcal{C}(E, \mathring{p}, \mathring{l})$). Differentiating $\mathcal{L}$ and using (33) and the fact that $\mathrm{tr}(\tilde{\Gamma}^\top([\tilde{\Gamma}, \Omega])) = 0$, one obtains

$$\begin{aligned} &\dot{\mathcal{L}} = \textstyle\sum_{i=1}^{n} k_i \mathring{p}_i^\top \pi_{e_{p_i}} (\Delta + \mathrm{Ad}_{\hat{H}} \tilde{\Gamma}) e_{p_i} \\ &- \textstyle\sum_{j=1}^{m} \kappa_j \mathring{l}_j^\top \pi_{e_{l_j}} (\Delta + \mathrm{Ad}_{\hat{H}} \tilde{\Gamma})^\top e_{l_j} + \mathrm{tr}(\mathrm{Ad}_{\hat{H}^{-1}} \Delta^\top \tilde{\Gamma}) \\ &= -\|\Delta\|^2 \leq 0, \end{aligned} \tag{35}$$

which is negative semi-definite and equal to zero when $\Delta = 0$. From there we will show next that there exists a local domain of initial conditions of $(E(0), \tilde{\Gamma}(0))$ so that Δ converges to zero and $(E(t), \tilde{\Gamma}(t))$ converge to $(I, 0)$.

Since the cost $\mathcal{C}(E, \mathring{p}, \mathring{l})$ involved in definition (34) of $\mathcal{L}$ is non-degenerate (see proof of Theorem 1) there exists an open neighbourhood of I in SL(3) where the cost $\mathcal{C}(E, \mathring{p}, \mathring{l})$ has compact connected sub-level sets containing the global minimum and no other critical point of the cost. Let $\mathfrak{B}^E \subset \mathrm{SL}(3)$ be such a sub-level set of the cost $\mathcal{C}(E, \mathring{p}, \mathring{l})$ on which the cost function $\mathcal{C}(E, \mathring{p}, \mathring{l})$ is proper with respect to E. Note that such a sub-level set $\mathfrak{B}^E$ exists since the Hessian $\mathrm{Hess}_1\mathcal{C}(I, \mathring{p}, \mathring{l})$ is positive definite. Note also that $\Delta = 0$ (or equivalently $\mathrm{grad}_1\mathcal{C}(E, \mathring{p}, \mathring{l}) = 0$) on $\mathfrak{B}^E$ implies that $E = I$. Since $\mathcal{L}$ is non-increasing as a consequence of (35), there exists a smaller subset $\mathfrak{B}_1^E \subset \mathfrak{B}^E$ and an open neighbourhood of the origin $\mathfrak{B}^{\tilde{\Gamma}} \subseteq \mathfrak{sl}(3)$ such that for all $(E(0), \tilde{\Gamma}(0)) \in \mathfrak{B}_1^E \times \mathfrak{B}^{\tilde{\Gamma}}$ one ensures that $E(t)$ remains in $\mathfrak{B}^E$ for all time.

Since Ω and H are bounded, one verifies that $\ddot{\mathcal{L}}$ remains bounded (i.e. $\dot{\mathcal{L}}$ is uniformly continuous) provided that $(E(0), \tilde{\Gamma}(0)) \in \mathfrak{B}_1^E \times \mathfrak{B}^{\tilde{\Gamma}}$. Direct application of Barbalat's lemma to (35) then ensures the asymptotic convergence of Δ to zero. This in turn implies that E converges to I since E remains in $\mathfrak{B}^E$ for all time.

From the expression (32) of $\dot{E}$ one deduces that $\ddot{E}$ is bounded. Then, using the fact that Δ converges to zero and E converges to I, it follows from Barbalat's lemma that $\lim_{t\to\infty} \dot{E} = -\mathrm{Ad}_{\hat{H}}\tilde{\Gamma} = 0$. Using the boundedness of H, one ensures the boundedness of $\hat{H}$ and $\hat{H}^{-1}$ and consequently the convergence of $\tilde{\Gamma}$ to zero. Finally the stability of the equilibrium $(E, \tilde{\Gamma}) = (I, 0)$ is a direct consequence of (34) and (35). ∎

Remark 1 *One verifies from* (30) *that* $(\hat{H}, \hat{\Gamma})$ *always evolve in* $\mathrm{SL}(3) \times \mathfrak{sl}(3)$ *using the fact that* $(\hat{H}(0), \hat{\Gamma}(0)) \in \mathrm{SL}(3) \times \mathfrak{sl}(3)$ *and the property* $\det(e^A) = e^{\mathrm{tr}(A)}$, $\forall A \in \mathbb{R}^{3\times 3}$. *In practice, however, to avoid numerical drift it is often desirable to enforce this constraint by frequently re-normalizing* $\hat{H}$ *and* $\hat{\Gamma}$ *onto* $\mathrm{SL}(3)$ *and* $\mathfrak{sl}(3)$*, respectively, using the projections* $\mathbb{P}_{\mathrm{SL}(3)}(\hat{H}) = \det(\hat{H})^{-\frac{1}{3}}\hat{H}$ *and* $\mathbb{P}_{\mathfrak{sl}(3)}(\hat{\Gamma}) = \hat{\Gamma} - \frac{1}{3}\mathrm{tr}(\hat{\Gamma})I$.

5 Experimental results – Image stabilization

In this section we present an application of the proposed approach to image stabilization in presence of very fast camera motion, severe occlusion, specular reflections, image blurring, and light saturation. The reported experiments have been conducted (using an Intel Core i7-6400 CPU running at 3.40Ghz) on datasets recorded by a prototype synchronized camera-IMU combination with an Aptina MT9V034 CMOS sensor and an Analog Devices ADIS16375 MEMS IMU. The IMU runs at 100 Hz, providing angular velocity measurements to the observer. The camera provides 20 frames per second at a resolution of 752×480 pixels.

• **Point-feature detection and matching:** The implemented code has been written in C++ with OpenCV library. Point-features are extracted using the `SurfFeatureDetector` routine with standard recommended parameter settings and matched using OpenCV's brute-force matcher `BFMatcher` routine with L_2-norm. It is quite unrealistic to track one and the same set of point-features through the long video sequence, in particular given the low frame rate and comparatively rapid motion in our test sequence as well as the presence of severe occlusion, specular reflections, poor image quality due to blur or light saturation. We have hence opted to match point-features between the reference image and each subsequent image frame separately. To do this, we first forward integrate the observer equations (30) using only the gyrometer measurements, i.e. setting the observer gains k_i $(i = 1, \cdots, n)$, κ_j $(j = 1, \cdots, m)$, and k_I to zero (i.e. **Prediction step** using (36)):

Prediction equations :

$$\begin{cases} \dot{\hat{H}}^+(t \in [t_{k-1}, t_k]) = \hat{H}^+([\Omega]_\times + \hat{\Gamma}^+) \\ \dot{\hat{\Gamma}}^+(t \in [t_{k-1}, t_k]) = [\hat{\Gamma}^+, [\Omega]_\times] \\ \hat{H}^+(t_{k-1}) = \hat{H}(t_{k-1}) \\ \hat{\Gamma}^+(t_{k-1}) = \hat{\Gamma}(t_{k-1}) \end{cases} \tag{36}$$

We then use the resulting predicted homography estimate $\hat{H}^+$ to transform the current image (i.e. warp the current image using the predicted homography $\hat{H}^+$ to obtain a prediction of the reference image) using the OpenCV's `warpPerspective` function before applying feature extraction and matching. The brute-force matching algorithm is well suited to this approach since it favors translational motion over rotational motion, and most of the rotational motion has already been compensated for by forward integrating the angular velocity.

To remove matched point-feature outliers, we first compute the standard deviation (sd_u, sd_v) and mean values (m_u, m_v) of the differences of coordinates in pixel (du_k, dv_k) of the point correspondences and then keep only those satisfying

$$\begin{cases} m_u - \max(sd_u, S) \leq du_k \leq m_u + \max(sd_u, S) \\ m_v - \max(sd_v, S) \leq dv_k \leq m_v + \max(sd_v, S) \\ |du_k| \leq D,\ |dv_k| \leq D \end{cases}$$

with S, D pre-defined positive thresholds ($S = 30$, $D = 80$ in our experiments). We have ***purposefully avoided*** the use of more sophisticated (and much more computationally expensive) alternative algorithms for outlier removal, such as RANSAC. Our simple and fast outlier removal method has yielded quite good matching results as for the test sequence there are either none or very few outliers (see Fig. 2 and the supplemental video).

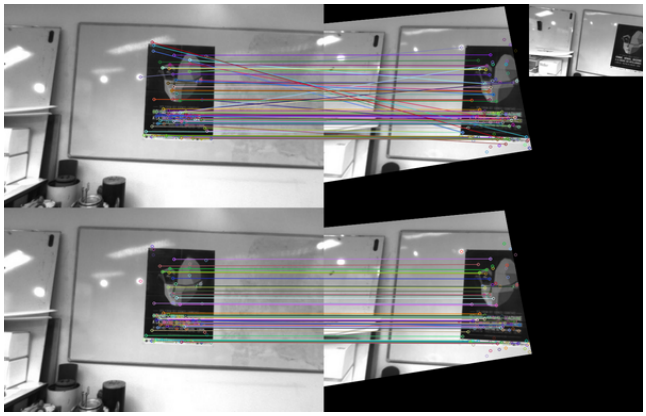

Fig. 2. Matching point correspondences between the warped image frame 264 (warped by the predicted homography) and the reference frame. **Poor matching (top) and excellent matching (bottom) before and after applying our outlier removal procedure.** Reference frame (left), warped current frame (right), current frame (small image on top right corner).

Fig. 3. Successful line matching between the image frame 169 (right) and the reference frame (left). Colorful points in both images are point correspondences used for our line matching algorithm.

• **Line-feature detection and matching:** Line-features are extracted using the probabilistic Hough transform (Matas, Galambos & Kittler 2000) with the OpenCV's `HoughLinesP` routine. Each extracted line in image coordinates (given by two points p_1^{im} and p_2^{im} in homogeneous coordinates) is then transformed into the line representation used in this paper (i.e., the normal to the plane containing the scene's line and the camera focal point) as

$$l = \frac{(K^{-1}p_1^{\text{im}}) \times (K^{-1}p_2^{\text{im}})}{|(K^{-1}P_1) \times (K^{-1}P_2)|} \in \mathbb{S}^2.$$

Matching two sets of lines of the reference image and the current image is more involved and has been scarcely developed in literature (and in OpenCV) compared to the point matching problem. We thus developed a simple line matching procedure which is described in (Hua, Trumpf, Hamel, Mahony & Morin 2017) but is omitted here due to space limitation. Excellent line matching results have been obtained for the reported test sequence (see Fig. 3 and the supplemental video).

• **Correction step of observer** (30)**:** After the steps of feature detection and matching, we use the observer gains of $k_i = 80$ $(i = 1, \cdots, n)$, $\kappa_j = 40$ $(j = 1, \cdots, m)$, $k_I = 0.05$ to rapidly iterate the observer equations (37) (i.e. the correction equations of observer (30)) 200 times per video frame (Note that the observer gains used for each iteration are divided by the number of iteration, i.e. using $\bar{k}_i = k_i/N_{iter}$, $\bar{\kappa}_j = \kappa/N_{iter}$ with $N_{iter} = 200$).

Correction equations :

$$\begin{cases} \hat{H}_{k+1} = \hat{H}_k \exp(-\bar{\Delta}_k T) \\ \hat{\Gamma}_{k+1} = \hat{\Gamma}_k - k_I \mathrm{Ad}_{\hat{H}_k^\top} \bar{\Delta}_k T \\ \bar{\Delta}_k = \left(-\sum_{i=1}^{n} \bar{k}_i \pi_{e_{pi}} \mathring{p}_i e_{pi}^\top + \sum_{j=1}^{m} \bar{\kappa}_j e_{lj} \mathring{l}_j^\top \pi_{e_{lj}} \right)_{\hat{H}=\hat{H}_k} \\ \hat{H}_0 \quad = \hat{H}^+(t_k), \quad \hat{\Gamma}_0 = \hat{\Gamma}^+(t_k) \end{cases} \tag{37}$$

with T the sampling time of the camera images. The computational effort for this last step is negligible compared to the previous image processing steps.

• **Performance evaluation:** The experimental results (cf. the video in the supplementary material and available at https://youtu.be/hlTkzjyENhg) show good and robust performance throughout the entire video sequence, including the previously mentioned passages with severe occlusion, specular reflection, poor image quality due to blur and/or light saturation (see Fig. 4). Even when temporarily no usable feature correspondence is available (e.g., frames 1148, 1391, 1593), or when our algorithm selects a wrong feature matching set (e.g., frames $1474 - 1488$, $1571 - 1581$) the observer continues to track the region of interest well and quickly recovers from any tracking errors.

To show the good performance and robustness of the proposed approach, we have carried out some more tests on datasets recorded on different lightning conditions and camera motions as shown in the following video links (1 indoor and 2 outdoor datasets):

• Indoor dataset: https://youtu.be/19lH0SaE-7Y
• Outdoor dataset ♯1: https://youtu.be/X-5hUOnesTo
• Outdoor dataset ♯2: https://youtu.be/dr_lo4xvuvw

6 Conclusions

The classical problem of homography estimation from point and line correspondences is the first time addressed with a nonlinear observer posed on the Special Linear group SL(3). The key advance of the proposed observer is the formulation of observer innovation that directly makes use of point and line correspondences from an image sequence without requiring explicit computation of the individual homographies between any two given images. Explicit observability conditions are established and the stability of the observer are proved for both cases of known full group velocity and partially known rigid-body velocities. A potential application to image stabilization in presence of very fast camera motion, severe occlusion, specular reflection, image blur, and light saturation is demonstrated with very encouraging results even for a relatively low video frame rate.

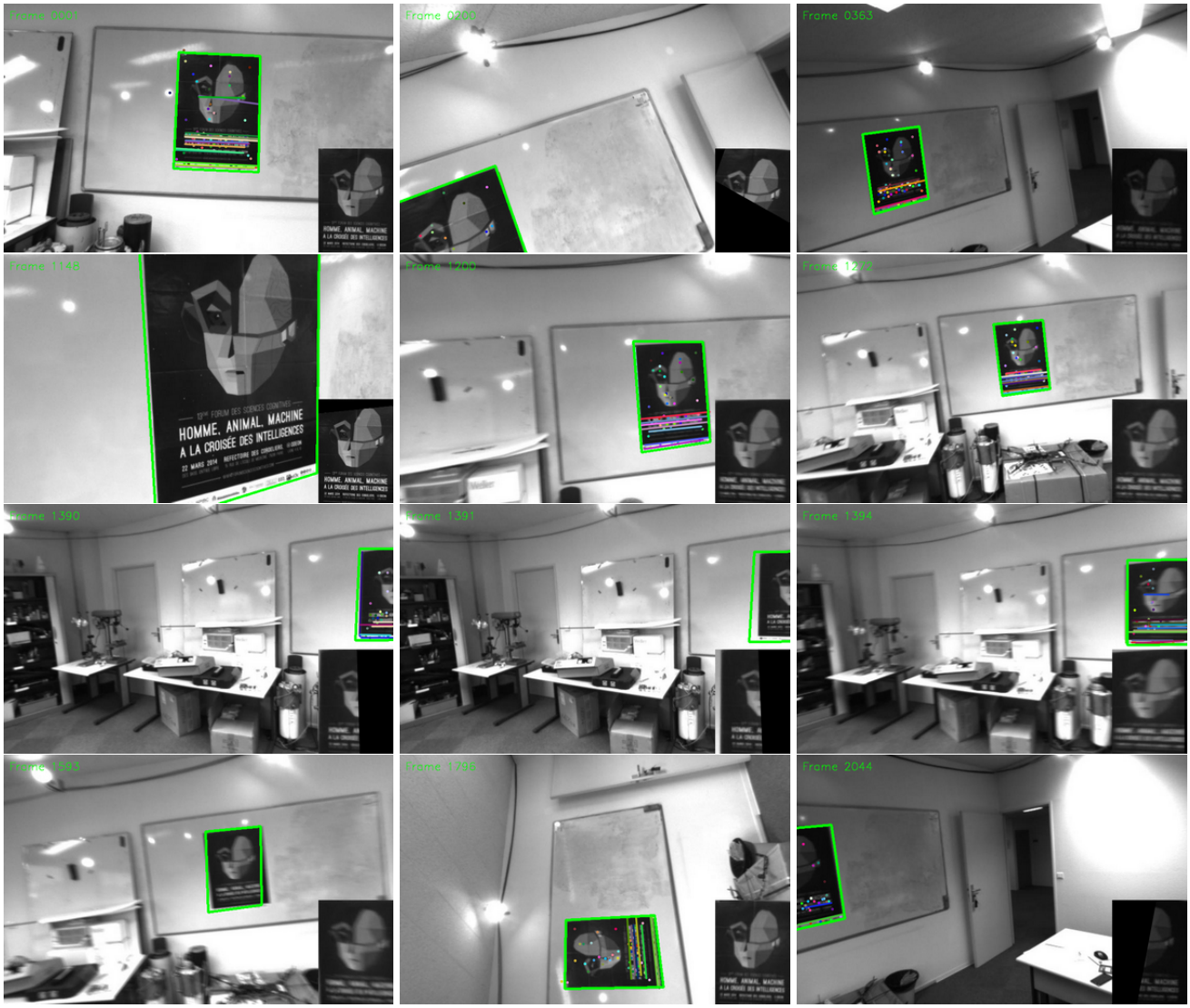

Fig. 4. **Good performance and robustness** of our algorithm for a very fast camera motion (relative to frame rate), and in presence of strong occlusion (e.g., frames 200, 1390, 2044), severe image blur (e.g., frames 1200, 1272, 1394, 1593) and light saturation (e.g., frame 363, 2044). The observer continues to operate even when temporarily no usable feature match is available (e.g., frames 1148, 1391, 1593). In each subplot of current frame, colorful points and lines are those successfully matched with the corresponding features in the reference image; and the green polygon represents a tracked region of interest (i.e., the poster) using the homography estimate. In the bottom right corner of each subplot, a crop of the warped current image is shown, telling us if the image is well stabilized or not. The full video of this experiment is available at https://youtu.be/hlTkzjyENhg.

References

Agarwal, A., Jawahar, C. & Narayanan, P. (2005). A survey of planar homography estimation techniques, *Technical Report IIIT/TR/2005/12*, IIIT, India.

Baldwin, G., Mahony, R., Trumpf, J., Hamel, T. & Cheviron, T. (2007). Complementary filter design on the Special Euclidean group SE(3), *European Control Conf. (ECC)*, pp. 3763–3770.

Barrau, A. & Bonnabel, S. (2015). An EKF-SLAM algorithm with consistency properties, *arXiv preprint arXiv:1510.06263* .

Barrau, A. & Bonnabel, S. (2017). The invariant extended kalman filter as a stable observer, *IEEE Trans. on Aut. Contr.* **62(4)**: 1797–1812.

Batista, P., Silvestre, C. & Oliveira, P. (2014). Attitude and earth velocity estimation-part II: Observer on the special orthogonal group, *IEEE Conf. on Dec. and Cont. (CDC)*, pp. 127–132.

Benhimane, S. & Malis, E. (2007). Homography-based 2D visual tracking and servoing, *Int. J. of Robotics Research* **26**(7): 661–676.

Berkane, S., Abdessameud, A. & Tayebi, A. (2017). Hybrid Attitude and Gyro-Bias Observer Design on SO(3), *IEEE Trans. on Automatic Control* **62**(11): 6044–6050.

Bhat, S. & Bernstein, D. (2000). A topological obstruction to continuous global stabilization of rotational motion and the unwinding phenomenon, *Systems & Control Letters* **39**(1): 63–70.

Bonnabel, S., Martin, P. & Rouchon, P. (2008). Symmetry-preserving observers, *IEEE Trans. on Automatic Control* **53**(11): 2514–2526.

Bonnabel, S., Martin, P. & Rouchon, P. (2009). Non-linear symmetry-preserving observers on Lie groups, *IEEE Trans. on Automatic Control* **54**(7): 1709–1713.

Caballero, F., Merino, L., Ferruz, J. & Ollero, A. (2007). Homography based Kalman filter for mosaic building. Applications to UAV position estimation, *IEEE Int. Conf. on Robotics and Automation (ICRA)*, pp. 2004–2009.

Conomis, C. (2006). Conics-based homography estimation from invariant points and pole-polar relationships, *IEEE Third Int. Symp. on 3D Data Processing, Visualization, and Transmission*, pp. 908–915.

de Plinval, H., Morin, P. & Mouyon, P. (2017). Stabilization of a class of underactuated vehicles with uncertain position measurements and application to visual servoing, *Automatica* **77**: 155–169.

Hamel, T., Mahony, R., Trumpf, J., Morin, P. & Hua, M.-D. (2011). Homography estimation on the Special Linear group based on direct point correspondence, *IEEE Conf. on Dec. and Cont. (CDC)*, pp. 7902–7908.

Hartley, R. & Zisserman, A. (2003). *Multiple View Geomerty in Computer Vision*, second edn, Cambridge University Press.

Hua, M.-D. (2010). Attitude estimation for accelerated vehicles using GPS/INS measurements, *Control Eng. Pract.* **18(7)**: 723–732.

Hua, M.-D., Hamel, T., Mahony, R. & Allibert, G. (2017). Explicit Complementary Observer Design on Special Linear Group SL(3) for Homography Estimation using Conic Correspondences, *IEEE Conf. on Dec. and Cont. (CDC)*, pp. 2434–2441.

Hua, M.-D., Trumpf, J., Hamel, T., Mahony, R. & Morin, P. (2017). Point and line feature-based observer design on SL(3) for Homography estimation and its application to image stabilization, *Technical Report hal-01628175*, I3S.

Hua, M.-D., Trumpf, J., Hamel, T., Mahony, R. & Morin, P. (2019). Feature-based recursive observer design for homography estimation and its application to image stabilization, *Asian Journal of Control* pp. 1–16.

Hua, M.-D., Zamani, M., Trumpf, J., Mahony, R. & Hamel, T. (2011). Observer design on the special euclidean group SE(3), *IEEE Conf. on Dec. and Cont. (CDC)*, pp. 8169–8175.

Izadi, M. & Sanyal, A. (2016). Rigid body pose estimation based on the lagrange-d'alembert principle, *Automatica* **71**: 78–88.

Jain, P. (2006). Homography estimation from planar contours, *IEEE Third Int. Symp. on 3D Data Processing, Visualization, and Transmission*, pp. 877–884.

Kaminski, J. & Shashua, A. (2004). Multiple view geometry of general algebraic curves, *Int. J. of Computer Vision* **56**(3): 195–219.

Khosravian, A., Trumpf, J., Mahony, R. & Hamel, T. (2016). State estimation for invariant systems on lie groups with delayed output measurements, *Automatica* **68**: 254–265.

Lageman, C., Trumpf, J. & Mahony, R. (2010). Gradient-like observers for invariant dynamics on a Lie group, *IEEE Trans. on Automatic Control* **55**(2): 367–377.

Lee, T., Leok, M., McClamroch, N. H. & Sanyal, A. (2007). Global attitude estimation using single direction measurements, *American Control Conference*, pp. 3659–3664.

Ma, Y., Soatto, S., Kosecka, J. & Sastry, S. (2003). *An Invitation to 3-D Vision: From Images to Geometric Models*, Springer Verlag.

Mahony, R. & Hamel, T. (2017). A geometric nonlinear observer for simultaneous localisation and mapping, *IEEE Conf. on Dec. and Cont. (CDC)*, pp. 2408–2415.

Mahony, R., Hamel, T., Morin, P. & Malis, E. (2012). Nonlinear complementary filters on the special linear group, *Int. J. of Control* **85**(10): 1557–1573.

Mahony, R., Hamel, T. & Pflimlin, J.-M. (2008). Nonlinear complementary filters on the Special Orthogonal group, *IEEE Trans. on Automatic Control* **53(5)**: 1203–1218.

Mahony, R., Trumpf, J. & Hamel, T. (2013). Observers for kinematic systems with symmetry, *9th IFAC Symposium on Nonlinear Control Systems*, pp. 617–633.

Malis, E., Chaumette, F. & Boudet, S. (1999). 2-1/2-D visual servoing, *IEEE Trans. on Robotics and Automation* **15**(2): 238–250.

Malis, E., Hamel, T., Mahony, R. & Morin, P. (2009). Dynamic estimation of homography transformations on the Special Linear group for visual servo control, *IEEE Int. Conf. on Robotics and Automation (ICRA)*, pp. 1498–1503.

Martin, P. & Salaün, E. (2008). An invariant observer for Earth-Velocity-Aided attitude heading reference systems, *IFAC World Congress*, pp. 9857–9864.

Matas, J., Galambos, C. & Kittler, J. (2000). Robust detection of lines using the progressive probabilistic hough transform, *Computer Vision and Image Understanding* **78(1)**: 119–137.

Nijmeijer, H. & (Eds.), T. F. (1999). *New Directions in Nonlinear Observer Design. Lect. Notes Control Informat. Sci.*, Vol. 244, New York: Springer-Verlag.

Rehbinder, H. & Ghosh, B. (2003). Pose estimation using line-based dynamic vision and inertial sensors, *IEEE Trans. on Autom. Control* **48**(2): 186–199.

Roberts, A. & Tayebi, A. (2011). On the attitude estimation of accelerating rigid-bodies using GPS and IMU measurements, *IEEE Conf. on Dec. and Cont. (CDC)*, pp. 8088—-8093.

Salcudean, S. (1991). A globally convergent angular velocity observer for rigid body motion, *IEEE Trans. on Automatic Control* **36**(12): 1493–1497.

Scaramuzza, D. & Siegwart, R. (2008). Appearance-guided monocular omnidirectional visual odometry for outdoor ground vehicles, *IEEE Trans. on Robotics* **24**(5): 1015–1026.

Shuster, M. (1978). Approximate algorithms for fast optimal attitude computation, *AIAA Guidance and Control Conference*, pp. 88–95.

Trumpf, J., Mahony, R., Hamel, T. & Lageman, C. (2012). Analysis of non-linear attitude observers for time-varying reference measurements, *IEEE Trans. on Automatic Control* **57(11)**: 2789–2800.

van Goor, P., Mahony, R., Hamel, T. & Trumpf, J. (2019). An equivariant observer design for visual localisation and mapping, *arXiv preprint arXiv:1904.02452* .

Vasconcelos, J., Cunha, R., Silvestre, C. & Oliveira, P. (2010). A nonlinear position and attitude observer on SE(3) using landmark measurements, *Systems & Control Letters* **59**: 155–166.

Wang, M. & Tayebi, A. (2017). Globally asymptotically stable hybrid observers design on $SE(3)$, *IEEE Conf. on Dec. and Cont. (CDC)*, pp. 3033–3038.

Wang, M. & Tayebi, A. (2019). Hybrid nonlinear observers for inertial navigation using landmark measurements, *arXiv preprint arXiv:1906.04689* .

Zlotnik, D. & Forbes, J. (2017). Nonlinear estimator design on the special orthogonal group using vector measurements directly, *IEEE Trans. on Automatic Control* **62(1)**: 149–160.